

Scalar quasinormal modes of a family of generalised Ellis–Bronnikov wormholes

Poulami Dutta Roy[#], S. Aneesh[†] and Sayan Kar^{#,**}

[#] *Department of Physics, Indian Institute of Technology Kharagpur, 721 302, India*

[†] *Department of Physics, 2001 Museum Road, P.O. Box 118440,*

University of Florida, Gainesville, FL 32611-8440 and

** Center for Theoretical Studies, Indian Institute of Technology, Kharagpur, 721 302, India*

Abstract

We obtain the scalar quasinormal modes (QNMs) in a family of Lorentzian wormholes proposed many years ago, as a generalisation of the well-known Ellis-Bronnikov spacetime. The effective potentials governing wave propagation, for different values of a metric parameter n and the angular momentum parameter m , show, in general, double-barrier features. However, for large m we do obtain potentials close to a single barrier. We use various methods to find the QNMs, eg. Prony-fit from the time-domain profile, direct integration and the semi-analytical WKB method. An agreement between the results, found by the two numerical methods, is achieved. The WKB results indicate, as expected, a deviation for small values of m and an agreement for large m , a fact demonstrated through our results. We also note the behaviour of the QNMs as a function of n (the metric parameter) and b_0 (the throat radius). The values of the QNM frequencies and damping time-constant for typical values of b_0 (multiples of the solar mass) are found. We conclude by noting how the shape of the wormhole, which is determined by the parameter n (and also by b_0) may be obtained from the nature and the values of the QNMs.

*Electronic address: poulamiphysics@iitkgp.ac.in, aneeshs@ufl.edu, sayan@phy.iitkgp.ac.in

I. INTRODUCTION

Much of the interest today in traversable Lorentzian wormhole spacetimes (originally proposed in [1], [2]) revolve around the question: *do they exist?* While the existence of black holes is no longer in doubt (more so after recent observations in M87 [3]), the wormhole story is far from complete. The same may also be said about naked singularities and cosmic censorship too [4].

The existence question on wormholes is based on a couple of issues. Firstly, classical General Relativity (GR) forbids them, stating that if the energy conditions on matter stress energy are to be believed as true, there are no wormholes [5–9]. In other words, the shape of the spatial slice of a wormhole is such that a converging null geodesic congruence would have to be defocused, as long as a throat and a ‘flare out to the other universe’ (second asymptotically flat region)– both necessary geometric features of wormholes–have to be admitted [10–12]. To get away with this so-called ‘defect’ or ‘problem’ one may appeal to modified theories of gravity. In such theories, the energy conditions on matter may hold but the convergence condition is violated [13], [14]. Examples of wormholes in modified gravity are numerous [15] and they largely have energy-condition-satisfying matter [16–26] and also sometimes non-phantom fields [27], [28]. In addition to taking refuge in modified gravity, we also know other ways of *restricting* the violation of energy conditions. These include dynamic wormholes [29], a proposal for limiting the amount of exotic matter [7] etc.

The second issue concerns possible signatures. Till recently, the most compelling signature for wormholes appeared to be using gravitational lensing [30]. However, with the advent of gravitational wave astronomy [31], one comes across the notion of *black hole mimickers* [32–35] (eg. wormholes, gravastars and other ultra-compact objects) which can ideally mimic the results found using black holes, in GW observations. In other words, one may, in some scenarios, be able to explain GW observations using such black hole mimickers as the end state of black hole and/or neutron star mergers [36]. Therefore, to improve upon viable templates for black hole mimickers, it is necessary to study various properties associated with them. One such property is a study of the quasinormal modes which can be used by observers at GW interferometers for verifying the wormhole proposal.

It is therefore of importance to study quasinormal modes of different types of wormhole spacetimes. This has been done to some extent in [37–44]. The main purpose of this article

is to further this line of thought through another class of ultra-static wormholes.

The choice of the family of wormholes we make here is based on an earlier paper [45] where the well-known Ellis-Bronnikov spacetime [46] had been extended to provide a two-parameter family of spacetimes. We study scalar QNMs in this family of wormholes. It may be asked—why only scalar QNMs? This is because they are the simplest to deal with. Another question which may be asked about our choice of spacetimes—do they exist as solutions in a theory of gravity? The answer to this not a direct ‘No’ because, we do expect the family of spacetimes to be a solution in a modified theory of gravity along the lines discussed in [47].

Our work in the paper is organised as follows. In Section II, we introduce the wormhole spacetime. We write down the Einstein tensor and equate it to the energy-momentum tensor of the ‘required matter’. Thereafter, we look at the energy conditions, embedding diagram and the extrinsic curvature tensor of spacelike slices. In Section III, we move on to studying scalar wave propagation in our wormhole background. Section IV gives a brief overview to all methods used for calculating quasinormal modes and Section V includes the results obtained from all methods and a comparison between them. It also discusses the interesting possibility of the QNMs being used as a tool to determine the shape of the wormhole geometry. Finally, in Section VI we end with our conclusions and comments.

II. THE GENERALISATION OF ELLIS-BRONNIKOV SPACETIME

In their 1973 papers [46], Ellis and Bronnikov constructed a spacetime where geometry is coupled to a phantom (negative kinetic energy) scalar field thus producing a static, spherically symmetric, geodesically complete, horizonless manifold with a throat (which he called a ‘drainhole’) connecting two asymptotically flat regimes. The line element of the spacetime constructed by Ellis and Bronnikov-

$$ds^2 = -dt^2 + \frac{dr^2}{1 - \frac{b_0^2}{r^2}} + r^2 d\theta^2 + r^2 \sin^2\theta d\phi^2. \quad (1)$$

where b_0 is the throat radius of the drainhole. Such a spacetime is known today as the Ellis-Bronnikov wormhole. If the Morris-Thorne conditions [5] necessary for the construction of a Lorentzian wormhole are considered then one finds that there is ample scope for various similar wormhole geometries to exist. Thus, a generalised version of the Ellis-Bronnikov wormhole geometry was suggested in [45] as a two-parameter (n and the throat radius b_0)

family of Lorentzian wormholes. When the parameter n takes the value $n = 2$, we get back the Ellis–Bronnikov spacetime. The motivation behind such a construction was to study the geodesics and propagation of scalar fields for a wider class of wormhole spacetimes and note various differences as well as similarities. The work also included the observation of resonances in the transmission coefficient for $n > 2$ geometries thus indicating that $n > 2$ geometries are distinctively different from the Ellis-Bronnikov geometry ($n = 2$). The line element of the generalised Ellis-Bronnikov spacetime involving the parameters n and b_0 is given as,

$$ds^2 = -dt^2 + d\ell^2 + r^2(\ell)d\theta^2 + r^2(\ell)\sin^2\theta d\phi^2 \quad (2)$$

where

$$r(\ell) = (\ell^n + b_0^n)^{1/n}. \quad (3)$$

The parameter n is allowed to take only even values to ensure the smooth behavior of $r(\ell)$ over the entire domain of the ‘tortoise’ or ‘proper radial distance’ coordinate ℓ ($-\infty \leq \ell \leq \infty$). The line element can also be written in an alternative form in terms of the usual radial coordinate r as,

$$ds^2 = -dt^2 + \frac{dr^2}{1 - \frac{b(r)}{r}} + r^2 d\theta^2 + r^2 \sin^2\theta d\phi^2 \quad (4)$$

where r and l are related through

$$dl^2 = \frac{dr^2}{1 - \frac{b(r)}{r}} \quad (5)$$

$$\Rightarrow b(r) = r - r^{(3-2n)}(r^n - b_0^n)^{(2-\frac{2}{n})}. \quad (6)$$

A. Geometry

Given the metric functions in eqn.(2), we note that the spacetime is spherically symmetric. All the metric components are independent of time and hence, all $t = \text{constant}$ slices are identical. This will be useful when we embed a 2-D slice of the wormhole in flat space, in order to understand its shape. The embedding diagram encodes the shape of the wormhole through a variation of the shape function $b(r)$ or $r(\ell)$ (w.r.t the ‘ ℓ ’ coordinate). Since $g_{tt} = -1$, the spacetime is ultra-static. It is easy to observe that the R_{00} component of the

Ricci tensor will always be zero for this family of wormholes, irrespective of the form of $r(\ell)$ and $b(r)$. The spacetime geometry owes such a behavior to the metric being ultra-static. We will see the distinction between different geometries for different n values explicitly when we plot the embedding diagram for different values of n and obtain the extrinsic curvature of the spacelike slices. One of the main objectives of this paper is to distinguish the different wormhole geometries for different values of n using the corresponding scalar quasi-normal modes.

B. Matter, energy conditions

The energy conditions are a way of ensuring that a solution of Einstein's equations is physically viable. The creation and maintenance of any traversable wormhole was first studied by Morris and Thorne [5] through the energy conditions that they are supposed to satisfy. It was observed that for a traversable wormhole to exist in GR the Weak Energy Condition (WEC) must be violated atleast at the throat. This meant that one requires *exotic matter* (i.e. matter violating the energy conditions). Later studies showed that all classes of static wormholes in GR need exotic matter for stability. This is a major drawback for wormholes and, as stated before, forbids their existence within the tenets of GR.

Let us now write down the energy-momentum tensor for our wormhole spacetime. This is done using the Einstein tensor and the Einstein equations. The energy-momentum tensor is defined by its diagonal components in the frame basis as $T_{00} = \rho(\ell)$, $T_{11} = \tau(\ell)$, $T_{22} = T_{33} = p(\ell)$ which turn out to be,

$$\rho(\ell) = \frac{1}{(b_0^n + \ell^n)^{2/n}} - \frac{\ell^{2n-2} + 2(n-1)b_0^n \ell^{n-2}}{(\ell^n + b_0^n)^2} \quad (7)$$

$$\tau(\ell) = \frac{\ell^{2n-2}}{(\ell^n + b_0^n)^2} - \frac{1}{(\ell^n + b_0^n)^{2/n}} \quad (8)$$

$$p(\ell) = \frac{(n-1)\ell^{n-2}b_0^n}{(\ell^n + b_0^n)^2} \quad (9)$$

in the units $8\pi G = c^2 = 1$. If we check the WEC inequalities: $\rho \geq 0$, $\rho + \tau \geq 0$ and $\rho + p \geq 0$, for the ρ , τ and p stated above, it can be seen that the second inequality is always violated for any value of parameters n and b_0 as well as ℓ . The other inequalities may not be violated for certain values of the parameters and the restricted domains of the ℓ coordinate. This can be observed more clearly when we plot $\rho(\ell)$, $\rho(\ell) + \tau(\ell)$ and $\rho(\ell) + p(\ell)$ with respect to

ℓ . We find that for some value of ℓ we do get matter with positive energy density, as can be seen from Fig.(1a). The third energy condition is also partially satisfied (see Fig.(1c)) but as already stated, the second energy condition is always violated (Fig.(1b)). Expectedly, violation of the WEC denotes the presence of exotic matter for the existence of this family of wormholes.

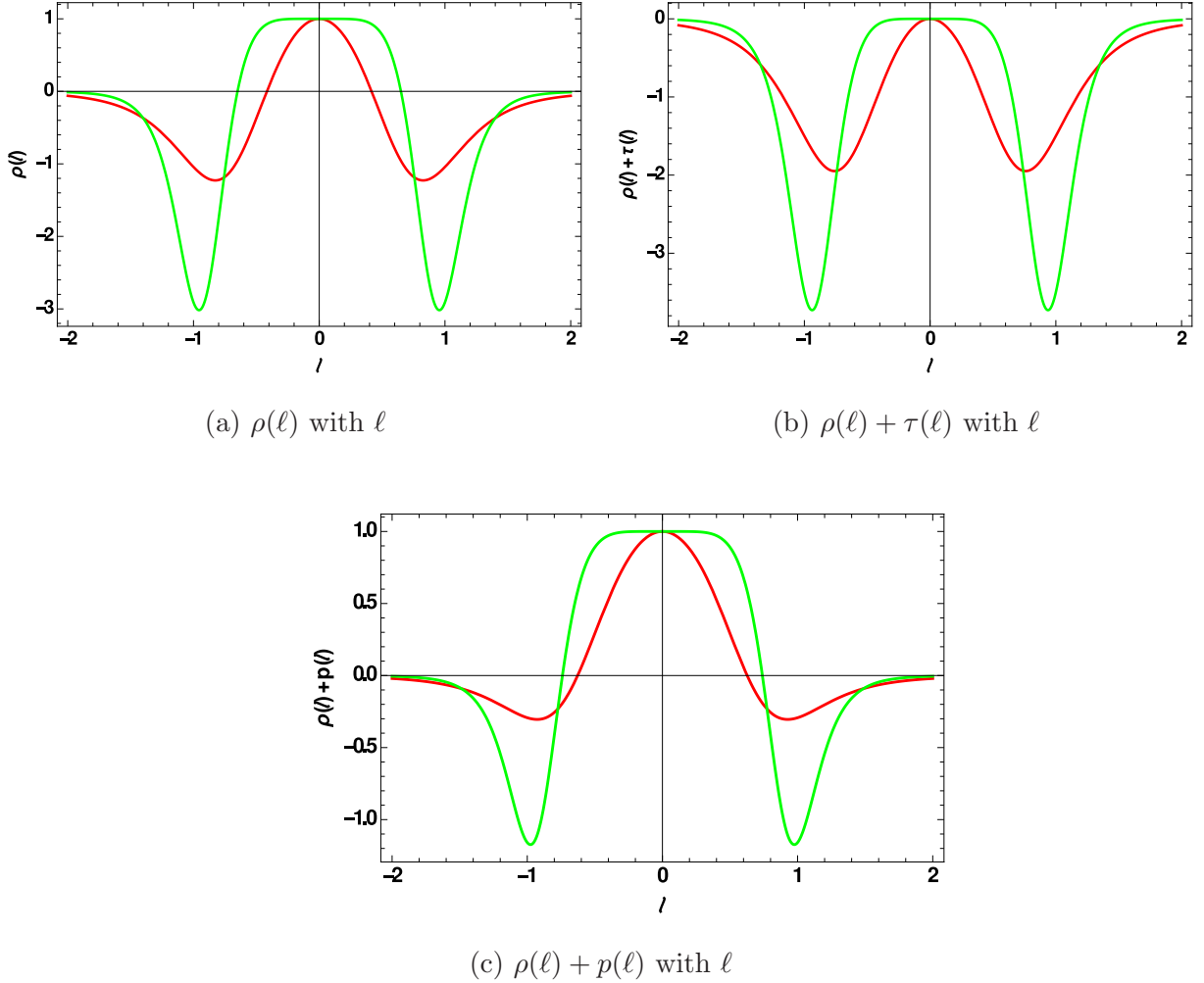


FIG. 1: Variation of $\rho(\ell)$, $\rho(\ell) + \tau(\ell)$ and $\rho(\ell) + p(\ell)$ with respect to ℓ . The red line is for $n = 4$ while the green one is for $n = 8$ geometry.

C. Embedding, extrinsic curvature

In order to visualise the shape of the generalised wormhole in 3+1 dimensions, for different values of n , the 2-D spatial slice ($t = \text{constant}$, $\theta = \pi/2$) of the spacetime is embedded in 3-D

Euclidean space with cylindrical coordinates. To begin with, we consider the $t = \text{constant}$, $\theta = \pi/2$ slice given as,

$$ds^2 = d\ell^2 + (\ell^n + b_0^n)^{2/n} d\phi^2. \quad (10)$$

The metric has now been reduced to a 2-D geometry which can be visualised by embedding it in a 3-D flat space. Since there is axial symmetry we use cylindrical coordinates (ρ, ψ, z) with the metric of the flat space being-

$$ds^2 = d\rho^2 + \rho^2 d\psi^2 + dz^2. \quad (11)$$

As the surface possesses axial symmetry, $\psi = \phi$, $z = z(\ell)$ and $\rho = \rho(\ell)$. Thus we get,

$$ds^2 = \left[\left(\frac{d\rho}{d\ell} \right)^2 + \left(\frac{dz}{d\ell} \right)^2 \right] d\ell^2 + \rho^2 d\phi^2. \quad (12)$$

Comparing this with eqn.(10) we find-

$$\rho(\ell) = (\ell^n + b_0^n)^{1/n} \quad (13)$$

$$\frac{dz}{d\ell} = \left(1 - (\ell^n + b_0^n)^{\frac{2}{n}-2} \ell^{2n-2} \right)^{1/2}. \quad (14)$$

The equation (14) is numerically integrated with $b_0 = 1$ and z is plotted with respect to ρ in a parametric plot giving the embedding diagram for different values of parameter n .

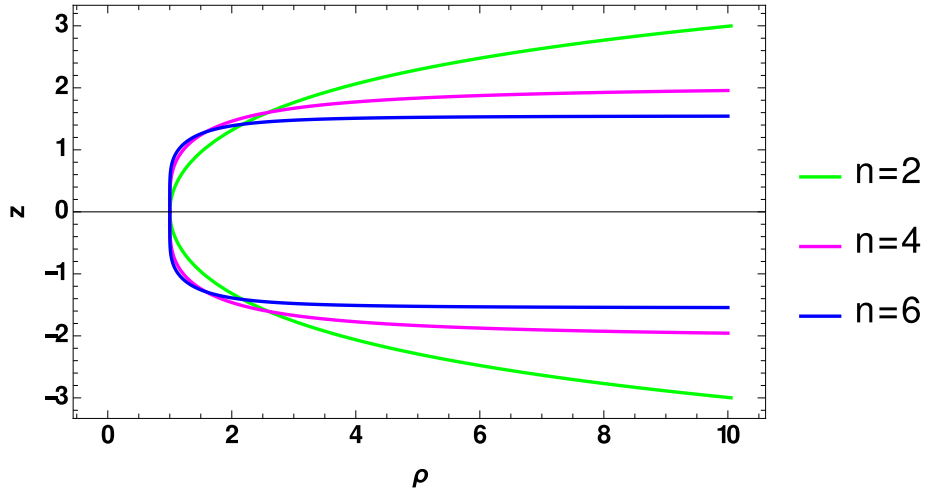


FIG. 2: Embedding diagram for different values of n .

As is evident in the plot of Fig.(2), the geometries for different n are quite distinct from each other. It is also observed that with increasing value of n the flaring out of the wormhole

gradually decreases. For larger n values it will become a uniform tunnel connecting two remote points within a single spacetime or points of two distinct spacetimes.

Once we have obtained the embedding, we can calculate the extrinsic curvature of the wormhole for different geometries as embedded in the above mentioned background. In order to compute the extrinsic curvature tensor we first need the tangents and normal to the wormhole. The tangent vector, with $x^i(\ell, \phi)$ as the embedding functions and g_{ij} as the background metric, is defined as follows,

$$e_\ell^i = \partial_\ell x^i, \quad e_\phi^i = \partial_\phi x^i. \quad (15)$$

Remembering the embedding functions (eqn.(13) and eqn.(14)) we get the two tangent vectors as-

$$e_\ell = (e_\ell^\rho, e_\ell^\psi, e_\ell^z) = (\partial_\ell \rho, 0, \partial_\ell z) = (\rho', 0, z') \quad (16)$$

$$e_\phi = (e_\phi^\rho, e_\phi^\psi, e_\phi^z) = (0, 1, 0). \quad (17)$$

There will only be one normal in our case and the components of the normal must satisfy

$$g_{ij} n^i n^j = 1, \quad g_{ij} n^i e_a^j = 0 \quad (18)$$

where $a = \ell, \phi$. Thus, a normal is obtained as

$$n = (n^\rho, n^\psi, n^z) = (-z', 0, \rho') \quad (19)$$

where prime denotes derivative with respect to ℓ . The extrinsic curvature tensor along the normal to the embedded wormhole is defined as

$$K_{ab} = -g_{ij} (e_a^k \nabla_k e_b^i) n^j \quad (20)$$

with the components being

$$K_{\ell\ell} = \rho'' z' - z'' \rho' = (n-1) b_0^n \ell^{n-2} (\ell^n + b_0^n)^{\frac{1-2n}{n}} (1 - \ell^{2n-2} (\ell^n + b_0^n)^{\frac{2}{n}-2})^{-1/2} \quad (21)$$

$$K_{\phi\phi} = -\rho z' = -(\ell^n + b_0^n)^{1/n} (1 - (\ell^n + b_0^n)^{\frac{2}{n}-2} \ell^{2n-2})^{1/2} \quad (22)$$

$$K_{\ell\phi} = K_{\phi\ell} = 0. \quad (23)$$

For $n = 2$ the trace of the tensor $g^{ij} K_{ij}$ is 0 indicating that the embedded surface for $n = 2$ geometry is extremal. In fact the $n = 2$ embedded surface is a catenoid.

III. SCALAR WAVE PROPAGATION AND QUASINORMAL MODES

We now consider the propagation of a massless, minimally coupled scalar field in our worm-hole spacetime (not necessarily a scalar field involved which may act as a source for the metric, but any generic scalar field) from which we intend to calculate the corresponding quasinormal modes. The QNMs will help us in understanding the stability of the spacetime under scalar perturbations and also give us an idea about whether we can distinguish the different geometries of the wormholes by simply looking at their QNMs.

We begin with the Klein-Gordon equation for the scalar field Φ -

$$\square\Phi = 0. \tag{24}$$

As our background spacetime is spherically symmetric and static we use the following ansatz to decompose Φ in terms of spherical harmonics, where the indices of $Y(\theta, \phi)$ have been suppressed for simplicity.

$$\Phi(t, r, \theta, \phi) = Y(\theta, \phi) \frac{\psi(r)e^{-i\omega t}}{r}. \tag{25}$$

Incorporating this in eqn.(24) we get the radial equation in the form of a Schrödinger-like equation in the tortoise coordinate,

$$\frac{d^2\psi}{d\ell^2} + [\omega^2 - V_{eff}]\psi = 0 \tag{26}$$

where

$$V_{eff}(\ell) = \frac{m(m+1)}{(b_0^n + \ell^n)^{2/n}} + \frac{(n-1)b_0^n \ell^{n-2}}{(b_0^n + \ell^n)^2} \tag{27}$$

where m is the angular momentum quantum number.

A. Effective potentials

If we compare equation (26) with Schrödinger-like equation we find that the term stated as V_{eff} in (26) acts as the effective potential. This effective potential depends on the parameter n and the angular momentum quantum number m . The potential will be different for each mode (m) for a specific geometry (n). The potential for all geometries is symmetric about

$l = 0$ and goes to zero at asymptotic limits. The effective potential can also be written in terms of the determinant of the extrinsic curvature tensor as described in eqns.(21–23):

$$V_{eff} = g^{\theta\theta}(m(m+1) - |K|) \quad (28)$$

where $|K| = -(n-1)b_0^n \ell^{n-2} (\ell^n + b_0^n)^{\frac{2}{n}-2}$ is the determinant of K_{ab} .

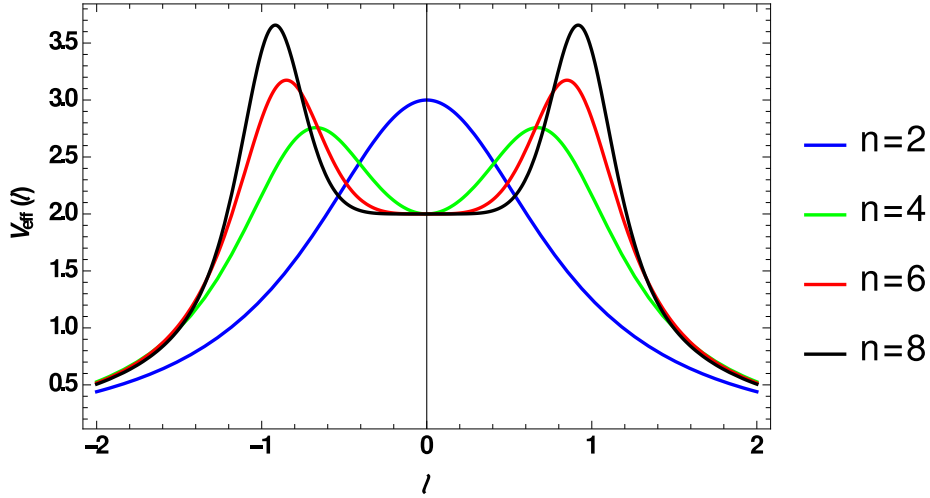


FIG. 3: Potentials for different values of n for $m = 1$.

There are certain remarks that need to be made on the effective potential:

- The plot in Fig.(3) shows the variation of $V_{eff}(\ell)$ w.r.t ℓ for different geometries at a particular value of $m = 1$. It can be seen that the potential has a single barrier feature only for $n = 2$, for all $n > 2$ there is a double barrier. This is true for *lower values of m*. Hence the $n > 2$ geometries are completely different from the Ellis-Bronnikov geometry.

- In Fig.(4), we find the potential being plotted once again for different geometries but with *higher m value*. It is interesting to observe that here the potential, for all geometries (i.e. for all $n > 2$), show a single barrier structure similar to the $n = 2$ case.

- The plot of the potential (Fig.(5)) for *higher n geometries* even for lower modes shows that although the potential is still a double barrier but the curves for different geometries are nearly identical.

When the scalar wave propagates it will experience such a potential due to the wormhole and hence if we detect such a wormhole, features of the effective potential must be reflected in the corresponding distribution of QNMs, when calculated for different modes and geometries.

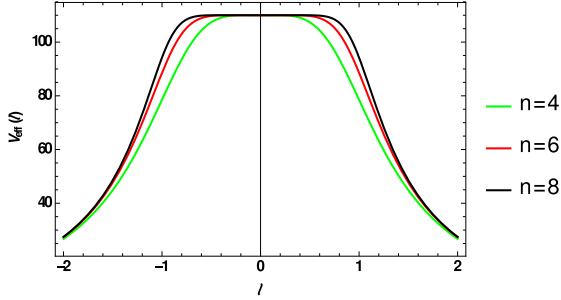


FIG. 4: Potentials for different values of n for $m = 10$.

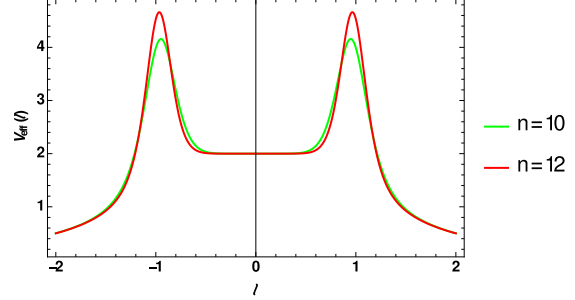


FIG. 5: Potentials for higher values of n and $m = 1$.

B. Time-domain profiles

The evolution of the scalar field with time can be observed through their time domain profiles. To obtain the profile we directly integrate the differential equation following the method described in [48] and [49]. We begin by writing the scalar wave equation in tortoise coordinates as

$$\frac{\partial^2 \psi}{\partial t^2} - \frac{\partial^2 \psi}{\partial \ell^2} + V_{eff}(\ell)\psi = 0. \quad (29)$$

Rewriting the equation in light cone coordinates $du = dt - d\ell$ and $dv = dt + d\ell$ we obtain,

$$\left(4\frac{\partial^2}{\partial u \partial v} + V(u, v)\right)\psi = 0. \quad (30)$$

The time evolution operator in light- cone coordinates can be written as

$$\begin{aligned} \exp\left(h\frac{\partial}{\partial t}\right) &= \exp\left(h\frac{\partial}{\partial u} + h\frac{\partial}{\partial v}\right) = \exp\left(h\frac{\partial}{\partial u}\right) + \exp\left(h\frac{\partial}{\partial v}\right) - 1 \\ &+ \frac{h^2}{2}\left(\exp\left(h\frac{\partial}{\partial u}\right) + \exp\left(h\frac{\partial}{\partial v}\right)\right)\frac{\partial^2}{\partial u \partial v} + \dots + O(h^4) \end{aligned} \quad (31)$$

Acting with this operator on ψ and incorporating eqn.(30) allows us to discretise the differential equation with step size, say, $h = 0.1$ and integrate along each rhombus built on two null surfaces $u = u_0$ and $v = v_0$. The initial conditions are defined on the lines $v = 0$ as a Gaussian profile centered at $u = 10$, $\psi(u, 0) = e^{-\frac{(u-10)^2}{100}}$ and on the $u = 0$ line as a constant, $\psi(0, v) = \text{constant}$, the value of which is determined by $\psi(0, 0)$. The plots below (Fig.(6a) and Fig.(6b)) show the time domain profiles for different geometries and modes. The typical QNM ringing pattern can be easily seen in the plots. As the mode number increases the intensity of the pattern also increases irrespective of geometry.

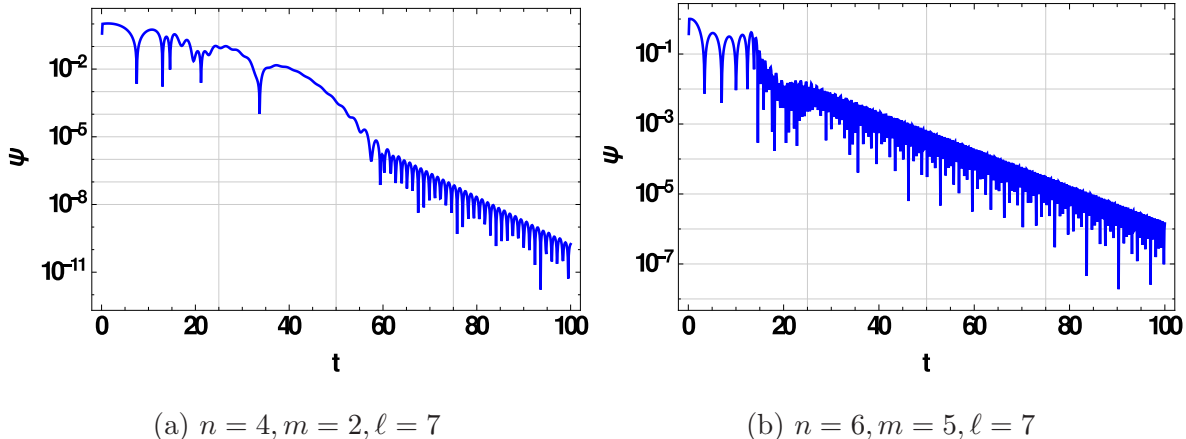


FIG. 6: Time domain profiles showing the characteristic QNM ringing.

IV. FINDING THE QUASINORMAL MODES

The scalar QNMs are obtained for different geometries using three different techniques. The method of Prony fitting and direct integration are completely numerical techniques while the WKB method is semi-analytic. In the following, we will discuss each method briefly and then move on to apply them for our WH.

A. Method I: Prony fit

The time domain profile can be used to obtain the corresponding QNMs by the Prony method of fitting the data via superposition of damped exponentials. We follow the procedure as discussed in [49]. We begin by writing ψ as a superposition of damped exponentials, i.e.

$$\psi(t) \approx \sum_{i=1}^p C_i e^{-i\omega_i t} \quad (32)$$

where p is the number of QNM frequencies that will fit the profile. If we assume the QNM ringing starts from $t = 0$ and continues till $t = Nh$ where N is an integer with $N \geq 2p - 1$, then each value of profile data can be written as

$$x_n \equiv \psi(nh) = \sum_{j=1}^p C_j e^{-i\omega_j nh} = \sum_{j=1}^p C_j z_j^n. \quad (33)$$

The Prony method allows us to find z_i in terms of known x_n and since h is also known, we can calculate the quasi-normal frequencies ω_i as

$$\omega_j = \frac{i}{h} \ln(z_j) \quad (34)$$

The values obtained can be checked by plotting them over the time domain profile and noting the fit.

B. Method II: Direct Integration

The method of direct integration, also called the shooting method, was developed by Chandrasekhar and Detweiler [50], where the differential equation (26) is directly integrated with the proper boundary conditions to obtain the QNMs. In our case, the potential is symmetric about $\ell = 0$ so the solutions can be divided into symmetric and antisymmetric classes. Hence the initial conditions for the two classes of QNMs will be: $\psi(0) = 0$ for antisymmetric solutions and $\psi'(0) = 0$ for symmetric solutions. Imposing this condition will help us in incorporating the behavior of ψ for negative values of ℓ as well. A similar treatment can be found for another wormhole geometry in [43]. Near the throat i.e. $\ell = 0, r = b_0$ we expand ψ as,

$$\psi = \sum_{n=0}^N B_{n/2} (r - b_0)^{n/2}; \quad r \rightarrow b_0 \quad (35)$$

We then write the coefficients $B_1, B_{3/2}, \dots$ in terms of B_0 and $B_{1/2}$. Also, ℓ can be expanded around $r = b_0$ as-

$$\ell = C_{1/2} (r - b_0)^{1/2} + C_1 (r - b_0)^1 + \dots \quad (36)$$

Hence,

$$\frac{d\psi}{d\ell} = \frac{B_{1/2}}{C_{1/2}} \quad (37)$$

Thus, for the symmetric solutions $B_{1/2} = 0$ while for the antisymmetric case $B_0 = 0$.

At infinity we similarly expand ψ in a series given as,

$$\psi = e^{i\omega\ell} \sum_{n=0}^N \frac{A_n}{r^n}; \quad r \rightarrow \infty. \quad (38)$$

We obtain the coefficients A_1, A_2, \dots in terms of A_0 . We integrate the differential equation (26) from b_0 to an arbitrary point r_0 . At r_0 the solution will have contribution from $e^{\pm i\omega\ell}$ terms.

$$\psi = e^{i\omega\ell} \sum_n \frac{A_n}{r^n} + e^{-i\omega\ell} \sum_n \frac{A'_n}{r^n} \quad (39)$$

Now, ψ can be written in terms of only A_0 and A'_0 . At the point r_0 , the integrated solution and the expansion (39) must match along with their derivatives. If we set the point r_0 to ∞ then as per the boundary condition of QNMs, only purely outgoing solutions will survive at infinity i.e. $A'_0 = 0$ which will give us the values of the QNM frequencies. The value of ω should be independent of the point of matching and hence must remain invariant over a range of values of r_0 . Also, the ratio of the amplitudes i.e. A'_0/A_0 must be ensured to be very close to zero at the ω_{QNM} value as it corresponds to a vanishing incoming wave at infinity. In this paper, we will refer only to the symmetric class of QNM frequencies which have low damping.

C. Method III: WKB

The semi-analytical method or WKB approximation was developed in the context of QNMs by Schutz and Will [51]. They calculated the QNM frequencies by taking the WKB solutions upto the eikonal limit which gives a simple analytical formula for the QNM frequencies containing only the parameters of the wormhole and the scalar field.

The QNM problem is considered as a scattering problem with the equation of the form-

$$\frac{d^2\psi}{dx^2} + Q(x)\psi = 0 \quad (40)$$

with $Q(x) = E - V(x)$.

The quantity $Q(x)$ is then expanded in Taylor series assuming that the turning points are close to the peak of the potential thus resulting in the parabolic shape of $Q(x)$ as shown in Fig.(7). The WKB solutions upto the eikonal limit are obtained for the regions I and III, while in region II the exact solution uses parabolic cylinder functions. The solutions for regions I and III are then matched simultaneously across both turning points with the asymptotic form of the exact solution of region II. This matching takes place only for a

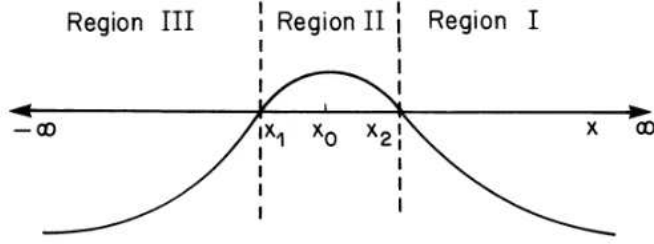


FIG. 7: The function: $(-)Q(x)$

discrete set of frequencies i.e. the QNM frequencies which also satisfy proper boundary conditions. The simple analytical formula obtained from the WKB method is given as-

$$\omega^2 = V_0 - i(p + \frac{1}{2})\sqrt{2V_0''}, \quad p = 0, 1, 2, \dots \quad (41)$$

where V_0 and V_0'' denotes the value of the potential and its second derivative at the point of maxima and p denotes the overtone number with $p = 0$ being the fundamental mode. In our work we will deal only with the fundamental modes and compare them with the numerical results.

Later the method was further developed by Iyer and Will to 3^{rd} order [52], by Konoplya upto 6^{th} order [53] and upto 13^{th} order by Matyjasek and Opala [54] which also included Padé approximation. For a recent comprehensive review on all the works on WKB one may refer to [55]. The WKB method is not a perturbative technique, hence higher orders may not necessarily ensure better results. In our case it has been observed that the WKB formula upto the eikonal limit gives better results than the higher order formulas. Also, one needs to keep in mind that the WKB formula used here is applicable for single barrier potentials i.e. when two turning points are involved. In our case though, for the lower modes with $n > 2$ we have a double barrier. Thus the WKB results will not be accurate. The formula needs to be suitably modified for four turning points in order to obtain better results.

V. COMPARING RESULTS FROM VARIOUS METHODS: AGREEMENTS, LIMITATIONS

We now calculate the QNMs using each of the above methods and compare the numerical results with the one obtained from the WKB method. For the calculations in this section we will take the throat radius $b_0 = 1$. The following two tables (Table I and Table II) list

the fundamental QNM values for different modes for the $n = 4$ and $n = 10$ geometry.

m	WKB	Prony	DI
1	1.79967-i 0.693811	1.66475-i 0.309338	1.69257-i 0.297442
2	2.59882-i 0.498842	2.64963-i 0.242272	2.65048-i 0.256227
3	3.52889-i 0.362154	3.63213-i 0.219813	3.62978-i 0.233729
5	5.49513-i 0.225716	5.62378-i 0.191588	5.60878-i 0.207342
7	7.49043-i 0.164178	7.6388-i 0.172743	7.59763-i 0.185464
10	10.4907-i 0.116874	10.7061-i 0.151295	10.5877-i 0.174096

TABLE I: Values of ω_{QNM} for different modes for $n = 4$.

m	WKB	Prony	DI
1	2.56783-i 1.56101	1.72679-i 0.189702	1.83676-i 0.38432
3	3.81611-i 1.06274	3.65001-i 0.110534	3.73325-i 0.246773
5	5.5703-i 0.601429	5.6289-i 0.079654	5.68859-i 0.192945
7	7.5017-i 0.276014	7.63526-i 0.0628301	7.64554-i 0.133035
10	10.4893-i 0.075948	10.6951-i 0.0473238	10.6214-i 0.109923

TABLE II: Values of ω_{QNM} for different modes for $n = 10$.

The plots of Fig.(8) show the difference in QNM values (denoted as $\Delta\omega$), between the two numerical methods when compared with the semi-analytic result i.e. the WKB method. With increasing m the difference decreases indicating a better match between analytical and numerical results. Before making a comment on which method is more suitable for calculating QNMs for a particular geometry (n value), one must keep in mind that the WKB result is important only for higher modes. In addition we note that it is an

approximate method and is not expected to give exact, accurate results. So the difference with WKB method will be a deciding factor only for higher modes. Also, the WKB method is applicable for a single barrier potential i.e. potential with two turning points. In our case, for $n > 2$ and for the lower modes, the effective potential is a double barrier and hence the WKB method is not suitable for lower modes in such geometries.

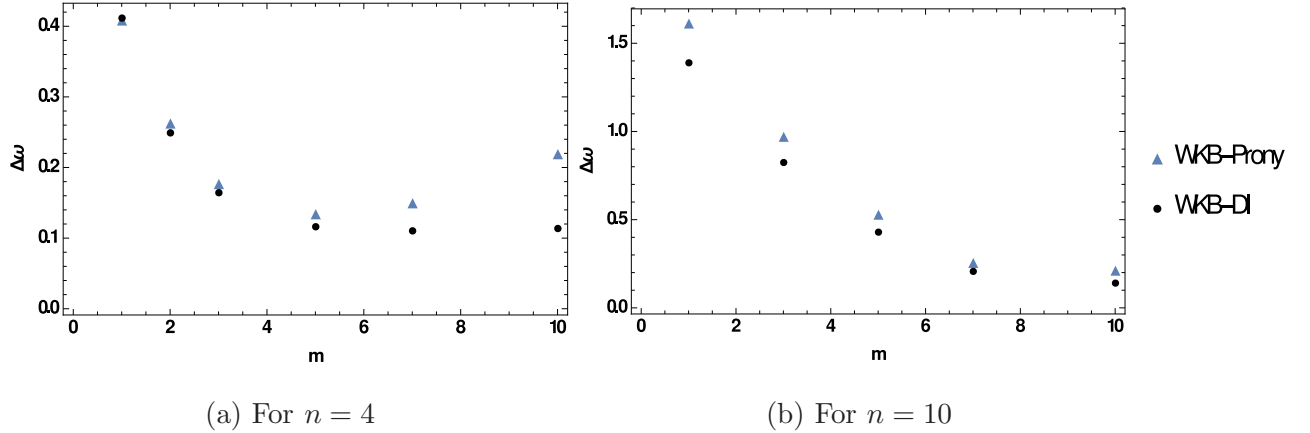


FIG. 8: Differences between QNMs from different methods

For geometries with lower n values

Observation: When a lower value of n is taken, we find that both the numerical methods give nearly the same result for lower modes, while at higher m , DI is better, as is evident from Fig.(8a).

Even though the plots in Fig.(8) show that DI-WKB difference is smaller compared to Prony-WKB, it does not necessarily make DI a better method for all cases, as WKB is an approximate method and exact results may differ from approximate ones.

Inference: For smaller n values, like 2, 4, 6, we find that when we consider lower modes (smaller m values) both numerical methods are equally suitable. On the contrary, when we go for higher modes, the DI method is more suited as the difference with the WKB values is lower than that for the Prony method.

For geometries with higher n values

Observation: While considering higher n values, one must keep in mind that even for lower m , the QNMs should be similar for different n , because of their nearly identical potentials as evident from Fig.(5). Even though we have not shown the results explicitly for $n = 8, 10, 12$, use of the DI method gives QNM values with very different imaginary parts which should not be the case.

Inference: For lower modes of higher n geometries, Prony method is better suited as the QNM values for different geometries are very close to each other, which matches with our above argument. For the higher modes, both numerical methods are equally suited for finding QNMs.

VI. WORMHOLE SHAPES FROM QNMS?

In this section we will explore the possibility of using QNMs as a tool to distinguish the different geometries corresponding to different values of n . The plot in Fig.(9) shows the variation of the real part of the fundamental ω_{QNM} with the magnitude of its imaginary part, for different values of n . Each point in the plot for a particular n corresponds to its QNM frequency for a particular angular momentum mode. As we move from left to right, the value of m goes on increasing, so the leftmost point corresponds to lowest m , while the rightmost point to the highest m . The QNM values have been calculated using the Prony method, a sample fit is shown in Fig.(10). From the plot of QNM frequencies in Fig.(9) we can draw the following conclusions:

- For lower n , the geometries are exactly distinguishable through their fundamental scalar QNMs.
- When we move on to higher n , the geometries start to look nearly identical as is evident from their QNMs (as well from their effective potentials Fig.(5)) for all modes and hence become difficult to distinguish.
- Note that lower modes are more suited for making comments about the geometries as for higher modes all geometries have similar QNM values due to their nearly identical single

barrier effective potential (see Fig.(4)).

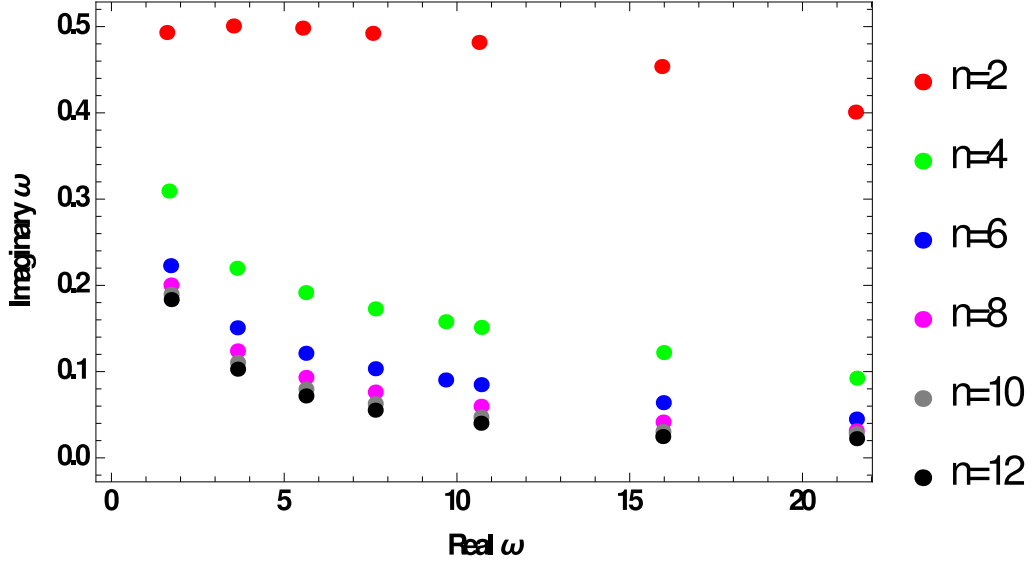


FIG. 9: Plot showing variation of real ω_{QNM} with the magnitude of its imaginary part for different n values. m increases from left to right for each n .

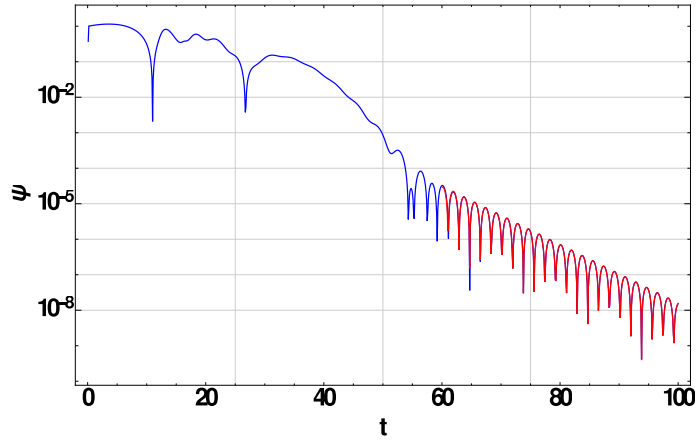


FIG. 10: Plot showing Prony fitting for $n = 10, m = 1$ where 3 frequencies have been fitted to the time domain profile.

A. Approximate Analytic Fit

In order to extract physically relevant information from our theoretical QNM values, we need an approximate model for ω which can be obtained by fitting the numerical results to analytical functions.

1. Fitting model for real part of ω

We intend to study the variation of frequency (obtained from the real part of ω) with throat radius for different geometries and modes. We observe from Table I and II that ω_r increases with increasing m . The value of ω_r also varies inversely with the throat radius. To imitate such a behavior we construct an approximate analytic model-

$$\omega_r = c \left(\frac{m + a n^d + g n^2 + h n^3 + k n^4 + p n^5}{b_0} \right) = c \left(\frac{f(n, m)}{b_0} \right) \quad (42)$$

where c is the speed of light, m is the corresponding mode which we want to fit, b_0 is in length units and the magnitudes of the constants a , d , g , h , k and p are obtained using the NonLinearModel fit in Mathematica, which fits the above model with frequency corresponding to each mode for each geometry calculated using the Prony method in Sec.V. For $m = 1$, $b_0 = 1$, $c = 1$ we get,

$$\omega_r = 1 + 0.604 n^{-0.268476} + 0.03903 n^2 - 0.008205 n^3 + 0.00065704 n^4 - 0.00001867 n^5. \quad (43)$$

For $m = 10$, fitting in the above model gives us,

$$\omega_r = 10 + 0.5456 n^{0.538566} - 0.05291 n^2 + 0.0082998 n^3 - 0.00056443 n^4 + 0.00001445 n^5. \quad (44)$$

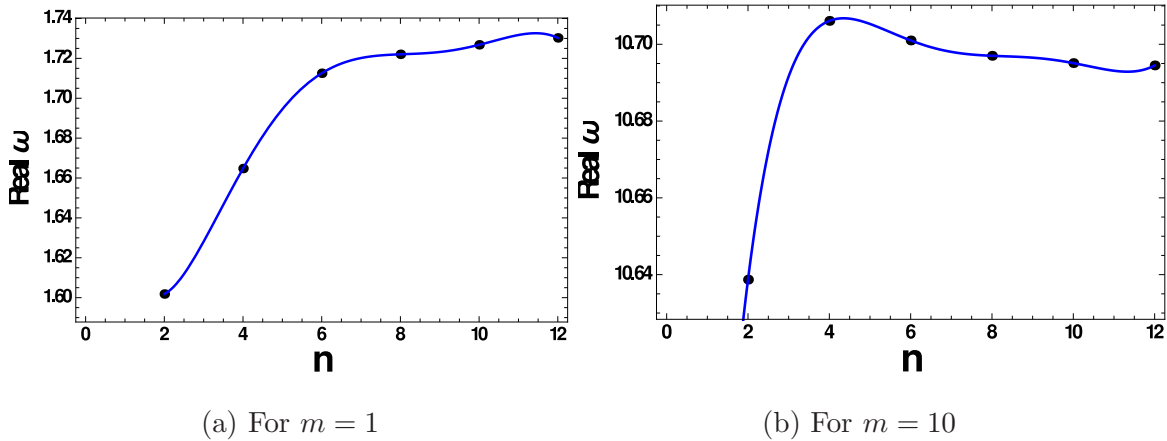


FIG. 11: Plot shows how well the real part of ω matches to the fit relation for different values of n . The smooth curve is the analytical fit with $b_0 = 1$, $c = 1$.

Writing the throat radius in units of M_\odot (which is physically meaningful) corresponding to each geometry we get,

$$\nu = \frac{f(n, m) c^3}{2 \pi b_0 G M_\odot} Hz \quad (45)$$

with $f(n, m)$ denoting the fitting function for each mode and geometry, $G = 6.67 \times 10^{-11} m^3 kg^{-1} s^{-2}$ and $M_\odot = 1.989 \times 10^{30} kg$.

2. Fitting model for imaginary part of ω

A similar analysis can also be done for the imaginary part of the QNM frequency whose inverse will give us the damping time. We fit the ω_i to a relation of n and m . We observe that the magnitude of ω_i decreases as m increases so we construct the approximate model as

$$\omega_i = c \left(\frac{a n^d + p n^2 + q n^3 + k n^4 + g n^5}{b_0 m} \right) = \frac{c F(n, m)}{b_0} \quad (46)$$

where c is again the speed of light, m is the corresponding angular momentum mode and the magnitudes of the constants a, d, p, q, k and g are to be determined from the NonLinear-Model fit of Mathematica. For $m = 1, c = 1, b_0 = 1$ we fit the frequency values as obtained from Prony fit method which gives the fitting function as

$$\omega_i = \frac{0.656637 n^{-0.175188} + 0.035808 n^2 + 0.00812771 n^3 - 0.000676108 n^4 + 0.0000196521 n^5}{1} \quad (47)$$

and for $m = 10$ we get

$$\omega_i = \frac{16.3911 n^{-1.78187} + 0.0191057 n^2 - 0.0038486 n^3 + 0.00029441 n^4 - 8.03737 \times 10^{-6} n^5}{10} \quad (48)$$

Hence the damping time will be given by a relation

$$\tau = \frac{2\pi}{|\omega_i|} = \frac{2 \pi b_0 G M_\odot}{c^3 F(n, m)}. \quad (49)$$

Using the above relation eq.(49) we can calculate some sample values of the damping time corresponding to different geometries for a fixed value of throat radius say $b_0 = 100M_\odot$ as shown in Table III. We observe that higher n geometries have larger damping time for the same value of throat radius.

n \ m	2	4	6	8	10	12
1	6.26	9.98	13.86	15.41	16.28	16.83
10	6.41	20.42	36.40	51.66	65.27	76.92

TABLE III: Values of $\tau(\times 10^{-3} sec)$ for different n corresponding to $m = 1$ and $m = 10$.

B. Variation of frequency with n and b_0 for constant m

We now try to find frequencies, using eq.(45), corresponding to a range of values of b_0 while keeping m fixed for each geometry. In Figs.(12a) and (12b), we observe that for almost the same range of throat radius, the frequencies corresponding to various geometries have higher values for higher modes. Hence, it is the lower modes that are more likely to be detected through the current generation of gravitational wave detectors, if wormholes exist in reality. In the case of higher m value, the frequency for different geometries are very similar corresponding to various throat radii. For lower modes though, the lower n geometries ($n = 2, 4, 6$) indeed have different frequencies for the same throat radius, thus making it possible to distinguish them.

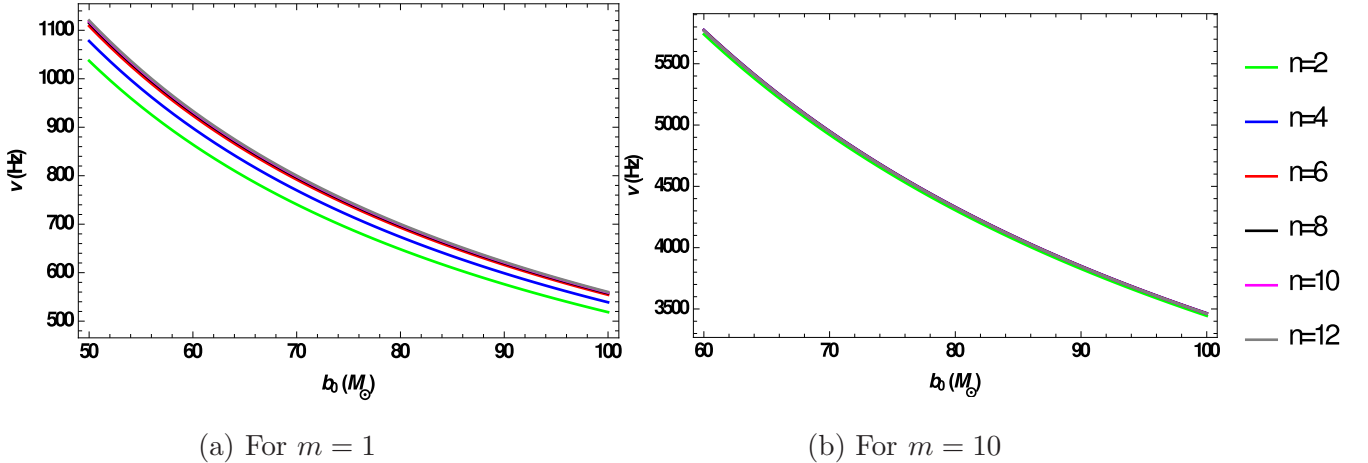


FIG. 12: Plot showing the variation of frequency for a range of values of b_0 corresponding to different geometries as obtained from the fitting relation in (45).

Apart from the plot, we can look at some sample values of frequency which will elaborate

on our above comment. Let us take the throat radius to be $b_0 = 70 M_\odot$ and once again using eq.(45) we will note the values of frequency for $m = 1$ and 10.

$n \backslash m$	2	4	6	8	10	12
1	740.76	769.86	791.96	796.35	798.55	800.16
10	4919.87	4951.04	4948.68	4946.83	4945.95	4945.67

TABLE IV: Values of ν in Hz for different n corresponding to $m = 1$ and $m = 10$.

As already mentioned, we observe from Table IV that for $m = 1$ the frequency for lower geometries are quite distinct from one another and hence the shape of the wormholes for different value of n can be easily identified from their lower mode QNMs. On the contrary, for $m = 10$ we find that the frequencies for all geometries are nearly identical and hence are not suitable for distinguishing the geometries. Thus, even if future detectors do succeed in detecting the higher modes, they would not help us in classifying the corresponding geometry of the wormhole from the frequency detected.

C. Variation of throat radius with n for constant ν and m

We can now look into the variation of the throat radius as a function of the other parameters namely, m , n and ν . As a sample case, we can take the frequency detected by GW detectors to be 500 Hz for the $m = 1$ mode, then the corresponding throat radius values in units of solar mass can be obtained (see Table V) using eqn.(45). We can easily notice that for higher n , the magnitude of b_0 becomes nearly identical. If we do the same calculation assuming 500 Hz for $m = 10$ mode (see Table V), all the geometries, except $n = 2$, give nearly identical values of b_0 . Also obtaining just the throat radius is not very useful in determining the shape of the wormhole, as wormholes can have different geometries while possessing the same throat radius (see Fig.(2)).

n \ m	2	4	6	8	10	12
1	103.707	107.781	110.874	111.489	111.798	112.022
10	688.781	693.145	692.815	692.556	692.433	692.394

TABLE V: Values of b_0 in units of M_\odot for different n corresponding to $m = 1$ and $m = 10$.

VII. CONCLUDING REMARKS

As mentioned right at the beginning, wormholes are shrouded in mystery ever since they were proposed (in their currently discussed incarnation) in the late 1980s. Studying the QNMs which may arise in perturbations of these exotic objects, gives us a new window to deal with their existence question. There are various existing (as well as exciting) theories and models describing wormholes. In our work, we have focused on the scalar quasinormal modes of individual members of one such family of Lorentzian wormholes. The character of this family of wormholes is that each member has a different geometry which is decided by the value of a parameter n , with $n = 2$ being the well-known Ellis-Bronnikov wormhole. The fact that the member wormholes of this family have different geometries can be easily visualised if one observes their shapes in embedding space. Through our work, we have tried to find a way to distinguish between the members in this wormhole family (each having a distinct shape), by obtaining and analysing the values and distributions of the corresponding fundamental scalar quasinormal modes, which may arise via scalar perturbations.

To begin with the task, we have first calculated the QNM frequencies for some members of the family using three methods: the WKB, Prony fitting and direct integration. While the WKB is semi-analytical, the other two methods are entirely numerical giving us better values of the QNM frequencies. After a brief overview of each method, we have calculated the QNMs and compared the numerical results with the semi-analytical ones. As expected, we find a better agreement of the numerical results with the WKB for higher angular momentum (m) values. Additionally, we have also commented on the suitability of each method in calculating the QNMs corresponding to different modes for each geometry. Since there are a number of methods available in the literature for computing QNMs, we need to know which

method is better suited for our spacetimes with a specific wormhole geometry (n value). Our results clearly indicate the most suitable method (out of the three we have studied) for computing QNMs for each individual geometry and angular momentum mode. Some of the interesting conclusions we have obtained are summarized in the following points:

- We observe that for members of the family with lower n value, both the Prony fit and the DI method are equally suitable in calculating QNMs for lower modes, while for higher m values the DI proves to be better.
- Next we look at the members of the family with higher value of n . We find that for lower modes the Prony method is better suited whereas for higher values of m , both numerical methods are equally suitable.
- The WKB method taken upto the eikonal limit is suitable for a single barrier potential, while in our case with $n > 2$ geometries for lower modes the potential has a double barrier structure. Thus the WKB method needs to be modified suitably whenever we have four turning points. We hope to address this issue later.

After identifying the appropriate numerical method for calculating QNMs for each member in both the high and low angular momentum values, we move on to investigating the possibility of distinguishing various members of the wormhole family through their corresponding QNMs for different modes. It is exciting to note that the geometries are indeed distinguishable from the observations of their fundamental QNMs alone. But this is true only for the wormholes with lower n values. For higher n , we cannot unfortunately make such a distinction about the shapes, as the geometries of all the wormholes become nearly identical making their distinction, just from their QNMs, difficult. This inability to distinguish is not a shortcoming of the methods used for calculating QNMs but rather is an innate feature present in this wormhole family. Note also that the QNMs corresponding to lower m values are better suited for distinguishing the geometries, as for higher modes the QNM values are similar for all geometries because of their similar effective potentials.

Finding a suitable source for this wormhole family with $n > 2$, by making the right choice of a modified theory of gravity, remains an unsolved issue left for the future. Hence, though we remain uncertain about the exact source producing such a wormhole family, it is nevertheless illuminating to study their QNMs, because of certain unique characteristic features (geometries, effective potentials and inter-connections), most of which may be obtained via a variation of the parameter ‘ n ’, which appears in the line element. Finally, in the dou-

ble barrier cases, it is likely that we will be able to obtain possible echo signals which are characteristically present in wormholes.

-
- [1] L. Flamm, *Beitrage zur einsteinschen gravitationstheorie*, Physikalische Zeitschrift **17**, 448 (1916); A. Einstein and N. Rosen, *The Particle Problem in the General Theory of Relativity*, Phys. Rev. **48**, 73 (1935).
 - [2] J. A. Wheeler, *Geons*, Phys. Rev. **97**, 511 (1955).
 - [3] The Event Horizon Telescope Collaboration, *First M87 Event Horizon Telescope Results. I. The Shadow of the Supermassive Black Hole*, Astro. J. Lett., Vol. **875**, no.1 (2019).
 - [4] R. Penrose, *Naked singularities*, Annals N.Y.Acad.Sci. **224**, 125-134 (1973); R. Penrose, *The question of cosmic censorship*, JAA, Vol. **20**, Issue 3–4, pp 233–248 (1999).
 - [5] M. Morris and K. S. Thorne, *Wormholes in spacetime and their use for interstellar travel: A tool for teaching general relativity*, Am. J. Phys., **56**, 395 (1988).
 - [6] M. Morris, K. S. Thorne; U. Yurtsever, *Wormholes, Time Machines, and the Weak Energy Condition*, Phys. Rev. Letts. **61**, 1446 (1988).
 - [7] M. Visser, S. Kar and N. Dadhich, *Traversable Wormholes with Arbitrarily Small Energy Condition Violations*, Phys. Rev. Lett. **90**, 201102 (2003).
 - [8] T. A. Roman, *Some Thoughts on Energy Conditions and Wormholes*, arXiv:gr-qc/0409090 (2004).
 - [9] F.S.N. Lobo (ed.), *Wormholes, Warp Drives and Energy Conditions*, Springer (2017).
 - [10] M. Visser, *Lorentzian wormholes: from Einstein to Hawking*, AIP Press (New York) 1995.
 - [11] S. W. Hawking and G. F. R. Ellis, *The large scale structure of spacetime*, Cambridge University Press.
 - [12] R. M. Wald, *General Relativity*, University of Chicago Press, First Indian Edition (2006).
 - [13] R. Shaikh, *Wormholes with nonexotic matter in Born-Infeld gravity*, Phys. Rev. **D 98**, 064033 (2018).
 - [14] F. Duplessis and D. A. Easson, *Traversable wormholes and non-singular black holes from the vacuum of quadratic gravity*, Phys. Rev.**D 92**, 043516 (2015).
 - [15] D. Hochberg, *Lorentzian wormholes in higher order gravity theories*, Phys. Letts. **B 251**, 349 (1990) ; B. Bhawal and S. Kar, *Lorentzian wormholes in Einstein-Gauss-Bonnet theory*, Phys.

- Rev **D 46**, 2464 (1992); A. G. Agnese and M. LaCamera, *Wormholes in the Brans-Dicke theory of gravitation*, Phys. Rev. **D 51**, 2011 (1995).
- [16] F.S.N. Lobo, *General class of wormhole geometries in conformal Weyl gravity*, Class. Quant. Grav. **25**, 175006 (2008), arXiv:0801.4401; G. U. Varieschi and K. L. Ault, *Wormhole geometries in fourth-order conformal Weyl gravity*, Int. J. Mod. Phys.**D 25**, 1650064 (2016).
- [17] M. K. Zangeneh, F. S. N. Lobo, and M. H. Dehghani, *Traversable wormholes satisfying the weak energy condition in third-order Lovelock gravity*, Phys. Rev.**D 92**, 124049 (2015).
- [18] A. Övgün, K. Jusufi, and I. Sakalli, *Exact traversable wormhole solution in bumblebee gravity*, Phys. Rev. **D 99**, 024042 (2019).
- [19] M. Zubair, F. Kousar and S. Bahamonde, *Static spherically symmetric wormholes in generalized $f(R, \phi)$ gravity*, EPJP **133**, 523 (2018).
- [20] F.S.N. Lobo and M.A. Oliveira, *Wormhole geometries in $f(R)$ modified theories of gravity*, Phys. Rev.**D 80**, 104012 (2009).
- [21] C.G. Böhmer, T. Harko and F.S.N. Lobo, *Wormhole geometries in modified teleparallel gravity and the energy conditions*, Phys. Rev.**D 85**, 044033 (2012).
- [22] R. Shaikh and S. Kar, *Wormholes, the weak energy condition, and scalar-tensor gravity*, Phys. Rev. **D 94**, no. 2, 024011 (2016).
- [23] E. Di Grezia, E. Battista, M. Manfredonia and G. Miele, *Spin, torsion and violation of null energy condition in traversable wormholes*, EPJP **132**: 537 (2017).
- [24] M. R. Mehdizadeh, M. K. Zangeneh and F. S.N. Lobo, *Einstein-Gauss-Bonnet traversable wormholes satisfying the weak energy condition*, Phys. Rev. **D 91**, 084004 (2015); H. Maeda and M. Nozawa, *Static and symmetric wormholes respecting energy conditions in Einstein-Gauss-Bonnet gravity*, Phys. Rev. **D 78**, 024005 (2008).
- [25] P. Kanti, B. Kleihaus, J. Kunz, *Wormholes in Dilatonic Einstein-Gauss-Bonnet Theory*, Phys.Rev.Lett. **107**, 271101 (2011); P. Kanti, B. Kleihaus, J. Kunz, *Stable Lorentzian wormholes in dilatonic Einstein-Gauss-Bonnet theory*, Phys.Rev.**D 85**, 044007 (2012).
- [26] R. Shaikh, *Lorentzian wormholes in Eddington-inspired Born-Infeld gravity*, Phys. Rev. **D 92**, 024015 (2015).
- [27] K. A. Bronnikov and A. M. Galiakhmetov, *Wormholes without exotic matter in Einstein-Cartan theory*, Grav. Cosmol. **21**, 283 (2015).
- [28] P. Cañate, J. Sultana and D. Kazanas, *Ellis wormhole without a phantom scalar field*, arXiv:

- 1907.09463/gr-qc (2019).
- [29] T. Roman, *Inflating Lorentzian wormholes*, Phys. Rev. **D 47**, 1370 (1993); S. Kar, *Evolving wormholes and the weak energy condition*, Phys. Rev. **D 49**, 862 (1994); S. Kar and D. Sahdev, *Evolving Lorentzian wormholes*, Phys. Rev. **D 53**, 722 (1996); D. Hochberg and M. Visser, *Null Energy Condition in Dynamic Wormholes*, Phys. Rev. Letts. **81** 746 (1998); D. Hochberg and M. Visser, *Dynamic wormholes, antitrapped surfaces, and energy conditions*, Phys. Rev. **D 58**, 044021 (1998).
- [30] J. G. Cramer, R. L. Forward, M. S. Morris, M. Visser, G. Benford and G. A. Landis, *Natural Wormholes as Gravitational Lenses*, Phys. Rev. **D 51**, 3117–3120 (1995); T. K. Dey and S. Sen, *Gravitational lensing by wormholes*, Mod. Phys. Letts. **A 13** (2008); R. Shaikh, P. Banerjee, S. Paul and T. Sarkar, *A novel gravitational lensing feature by wormholes*, Phys. Letts. **B**, Vol. **789** pp. 270–275 (2019).
- [31] B. P. Abbott et. al, *GW170817: Observation of Gravitational Waves from a Binary Neutron Star Inspiral*, Phys. Rev. Letts. **119**, 161101 (2017); B. P. Abbott et al., *GW151226: Observation of Gravitational Waves from a 22-Solar-Mass Binary Black Hole Coalescence*, Phys. Rev. Letts. **16**, 241103 (2016); B. P. Abbott et al., *GW170104: Observation of a 50-Solar-Mass Binary Black Hole Coalescence at Redshift 0.2*, Phys. Rev. Letts. **118**, 221101 (2017); B. P. Abbott et al., *GW170608: Observation of a 19-solar-mass Binary Black Hole Coalescence*, Astrophys. J. **851**, no. 2, L35 (2017); B. P. Abbott et al., *GW170814: A Three-Detector Observation of Gravitational Waves from a Binary Black Hole Coalescence*, Phys. Rev. Letts. **119**, 141101 (2017); B. P. Abbott et. al., *Binary Black Hole Mergers in the first Advanced LIGO Observing Run*, Phys. Rev. **X 6**, 041015 (2016).
- [32] J.P. S. Lemos and O. B. Zaslavskii, *Black hole mimickers: regular versus singular behavior*, Phys. Rev. **D 78** : 024040 (2008); P. Pani, V. Cardoso, M. Cadoni and M. Cavaglia, *Ergoregion instability of black hole mimickers*, Proc. of Sc. (BHs, GR and Strings): **027** (2008); V. Cardoso and P. Pani, *Testing the nature of dark compact objects: a status report*, arXiv:1904.05363v3 [gr-qc] (2019).
- [33] T. Damour and S.N. Solodukhin, *Wormholes as black hole foils*, Phys. Rev. **D 76**, 024016 (2007); R. A. Konoplya, A. Zhidenko, *Wormholes versus black holes: quasinormal ringing at early and late times*, JCAP **12** ,043 (2016); R. N. Izmailov, A. Bhattacharya, E. R. Zhdanov, A. A. Potapov and K. K. Nandi, *Can massless wormholes mimic a Schwarzschild black hole*

- in the strong field lensing?*, Eur. Phys. J Plus **134**: 384 (2019).
- [34] F. S. Guzman and J. M. Rueda-Becerril, *Spherical Boson Stars as Black Hole mimickers*, Phys. Rev. D **80** (2009) 084023, arXiv:1009.1250v1 [astro-ph.HE]; F. S. Guzman, *Accretion disc onto boson stars: A Way to supplant black holes candidates*, Phys. Rev. D **73**, 021501 (2005); D. F. Torres, S. Capozziello and G. Lambiase, *A supermassive boson star at the galactic center?*, Phys. Rev. D **62**, 104012 (2000).
- [35] P. O. Mazur and E. Mottola, *Gravitational Condensate Stars: An Alternative to Black Holes*, LA-UR-01-5067, arXiv:gr-qc/0109035v5 (2002); P. Pani, E. Berti, V. Cardoso, Y. Chen and R. Norte, *Gravitational-wave signature of a thin-shell gravastar*, J. Phys.: Conference Series, Vol. **222**, No. 1 (2010); K. Glampedakis and G. Pappas, *How well can ultracompact bodies imitate black hole ringdowns?*, Phys. Rev. D **97** (2018) no.4, 041502, arXiv:1710.02136v2 [gr-qc].
- [36] N. V. Krishnendu, K. G. Arun, C. K. Mishra, *Testing the binary black hole nature of a compact binary coalescence*, Phys. Rev. Lett. **119**, 091101 (2017); V. Cardoso, S. Hopper, C. F. B. Macedo, C. Palenzuela and Paolo Pani, *Echoes of ECOs: gravitational-wave signatures of exotic compact objects and of quantum corrections at the horizon scale*, Phys. Rev. D **94**, 084031 (2016)
- [37] R. A. Konoplya and A. Zhidenko, *Wormholes versus black holes: quasinormal ringing at early and late times*, JCAP **12**, 043 (2016); R. A. Konoplya and A. Zhidenko, *Passage of radiation through wormholes of arbitrary shape*, Phys. Rev. D **81**, 124036 (2010).
- [38] R. A. Konoplya, *How to tell the shape of a wormhole by its quasinormal modes*, Phys. Letts. **B**, Vol. **784** pp. 43–49 (2018).
- [39] P. Bueno, P. A. Cano, F. Goelen, T. Hertog and B. Vercknocke, *Echoes of Kerr-like wormholes*, Phys. Rev. D **97**, 024040 (2018).
- [40] S. Kim, *Wormhole perturbation and its quasi-normal modes*, Prog. Theo. Phys. Suppl., No. **172**, 21 (2008).
- [41] R. A. Konoplya and C. Molina, *Ringing wormholes*, Phys. Rev. D **71**, 124009 (2005).
- [42] S. H. Volölkel and K. D. Kokkotas, *Wormhole Potentials and Throats from Quasi-Normal Modes*, Class. Quant. Grav. **35**, no. 10, 105018 (2018).
- [43] S. Aneesh, S. Bose and S. Kar, *Gravitational waves from quasinormal modes of a class of Lorentzian wormholes*, Phys. Rev. D **97**, 124004 (2018).
- [44] J. L. Blázquez-Salcedo, X. Y. Chew and J. Kunz, *Scalar and axial quasinormal modes of*

- massive static phantom wormholes*, Phys. Rev. **D 98**, 044035 (2018).
- [45] S. Kar, S.N. Minwalla, D. Mishra and D. Sahdev, *Resonances in the transmission of massless scalar waves in a class of wormholes*, Phys. Rev. **D Vol.51** , No. **4** (1994).
- [46] H. G. Ellis, J. Math. Phys. **14**, 104 (1973); Erratum-ibid. **15**, 520 (1974); K. A. Bronnikov, Acta Phys. Polon. **B 4**, 251 (1973). T. Kodama, Phys. Rev. **D 18**, 3529 (1978); H. G. Ellis, Gen. Relativ. Grav. **10**, 105 (1979).
- [47] S. Kar, S. Lahiri and S. SenGupta, *Can extra dimensional effects allow wormholes without exotic matter?*, Phys. Letts. **B**, Vol. **750** pp. 319–324 (2015).
- [48] C. Gundlach, R. Price and J. Pullin, *Late-time behavior of stellar collapse and explosions.I. Linearized perturbations*, Phys. Rev. **D 49** ,883 (1994).
- [49] R.A. Konoplya and A. Zhidenko, *Quasinormal modes of black holes: from astrophysics to string theory*, Rev. Mod. Phys. **83**, 793 (2011).
- [50] S. Chandrasekhar and S. Detweiler, *The quasi-normal modes of the Schwarzschild black hole*, Proc. R. Soc. Lond. **A 344**,441 (1975).
- [51] B. F. Schutz and C. M. Will, *Black hole normal modes - a semi-analytic approach*, Astrophys. J., **L291**, 33 (1985).
- [52] S. Iyer and C.M. Will, *Black-hole normal modes: A WKB approach. I. Foundations and application of a higher-order WKB analysis of potential-barrier scattering*, Phys. Rev. D **35**, 3621 (1987).
- [53] R. A. Konoplya, *Quasinormal behavior of the D-dimensional Schwarzschild black hole and higher order WKB approach*, Phys. Rev. D **68**, 024018 (2003).
- [54] J.Matyjasek and M. Opala, *Quasinormal modes of black holes. The improved semianalytic approach*, Phys. Rev. D **96**, 024011 (2017).
- [55] R. A. Konoplya, A. Zhidenko and A. F. Zinhailo, *Higher order WKB formula for quasinormal modes and grey-body factors: recipes for quick and accurate calculations*, arXiv:1904.10333 [gr-qc].